

lubrication: At the start-up of motion, yield occurs within the thin liquid film rather than by the degradation of solid surfaces.

REFERENCES AND NOTES

1. I. L. Singer and H. M. Pollock, Eds., *Fundamentals of Friction* (Kluwer Academic, Dordrecht, Netherlands, 1992).
2. J. N. Glosli and G. M. McClelland, *Phys. Rev. Lett.* **70**, 1960 (1993).
3. B. N. J. Persson, *ibid.* **71**, 1212 (1993).
4. H. Yoshizawa, P. McGuiggan, J. Israelachvili, *Science* **259**, 1305 (1993); M. L. Gee, P. M. McGuiggan, J. N. Israelachvili, *J. Chem. Phys.* **93**, 1895 (1990).
5. S. Granick, *Science* **253**, 1374 (1991).
6. F. W. Smith, *Wear* **2**, 250 (1959).
7. S. Bair and W. O. Winer, *J. Tribology* **114**, 1 (1992), and references therein.
8. C. R. Evans and K. L. Johnson, *Proc. R. Soc. London Ser. A* **356**, 215 (1977), and references therein.
9. J. N. Israelachvili and P. M. McGuiggan, *Science* **241**, 795 (1988).
10. J. Van Alsten and S. Granick, *Phys. Rev. Lett.* **61**, 2570 (1988).
11. J. Peachey, J. Van Alsten, S. Granick, *Rev. Sci. Instrum.* **62**, 463 (1991).
12. H.-W. Hu, thesis, University of Illinois at Urbana-Champaign (1992).
13. J. D. Ferry, *Viscoelastic Properties of Polymers* (Wiley, New York, ed. 3, 1980).
14. M. Schoen, C. L. Rhykerd, D. J. Diestler, J. H. Cushman, *Science* **245**, 1223 (1989).
15. P. A. Thompson and M. O. Robbins, *ibid.* **250**, 792 (1990).
16. P. A. Thompson, G. S. Grest, M. O. Robbins, *Phys. Rev. Lett.* **68**, 3448 (1992).
17. H. Yoshizawa and J. Israelachvili, *J. Phys. Chem.* **97**, 11300 (1993).
18. H.-W. Hu and S. Granick, *Science* **258**, 1339 (1992).
19. M. de Sousa Vieira, G. L. Vasconcelos, S. R. Nagel, *Phys. Rev. E* **47**, R2221 (1993), and references therein.
20. S. Onogi, T. Masuda, T. Matsumoto, *Trans. Soc. Rheol.* **14**, 275 (1970).
21. C. R. Kessel and S. Granick, *Langmuir* **7**, 532 (1991).
22. H. M. Jaeger and S. R. Nagel, *Science* **255**, 1523 (1992).
23. M. J. Adams, in (1), pp. 183–207.
24. B. J. Ackerson and N. A. Clark, *Phys. Rev. Lett.* **46**, 123 (1981).
25. L. B. Chen *et al.*, *ibid.* **69**, 688 (1992), and references therein.
26. M. J. Stevens, M. O. Robbins, J. F. Belak, *ibid.* **66**, 3004 (1991).
27. Discontinuities of this kind were also observed for linear alkanes (undecane and dodecane), methylundecane, and the globular-shaped molecule octamethylcyclotetrasiloxane (OMCTS). The significance of the control experiment with OMCTS was to show that a conceivable coil stretch of the chain-like molecules could not explain the yield transition in general.
28. R. M. Overney *et al.*, *Nature* **359**, 133 (1992), and references therein.
29. We dedicate this paper to David Tabor on the occasion of his 80th birthday. We thank B. Cabane, J. D. Ferry, J. N. Israelachvili, K. Johnson, and J. Klein for discussions; C. R. Kessel, J. Peanasky, and L. Cai for assistance with measurements involving OTE monolayers; and W. R. Jones of the National Aeronautics and Space Administration–Lewis Space Center for donating the PFG. Supported by the Exxon Corporation and by the taxpayers of the United States through grants from the National Science Foundation (Tribology Program, NSF-MSM-92-02143) and the Air Force Office of Scientific Research (AFOSR-URI-F49620-93-1-02-41).

23 September 1993; accepted 31 January 1994

Defects in Carbon Nanostructures

O. Zhou, R. M. Fleming, D. W. Murphy, C. H. Chen, R. C. Haddon, A. P. Ramirez, S. H. Glarum

Previous high-resolution electron microscopy (HREM) observations of the carbon nanotubes have led to a “Russian doll” structural model that is based on hollow concentric cylinders capped at both ends. The structures of the carbon nanotubes and particles were characterized here by bulk physical and chemical property measurements. The individual nanostructure is as compressible as graphite in the *c* axis, and such nanostructures can be intercalated with potassium and rubidium, leading to a saturation composition of “MC₈.” These results are counter to expectations that are based on a Russian doll structure. HREM after intercalation with potassium and deintercalation indicates that individual nanoparticles are a “paper-mache” of smaller graphite layers. Direct current magnetization and electron spin resonance measurements indicate that the electronic properties of the nanostructures are distinctly different from those of graphite. Although the nanostructures have distinct morphologies and electronic properties, they are highly defective and have a local structure similar to turbostratic graphite.

Modification of the spark erosion technique (1, 2) for the synthesis of fullerenes has led to the discovery (3) and preparation of macroscopic quantities of carbon nanotubes (4). HREM images have been used to construct a model based on hollow concentric cylinders capped at both ends by curved sections (3, 4). Concentric, almost spherical nanoparticles (onions) with hollow centers are also formed along with the tubes during spark erosion. Similar spherical nanoparticles are formed upon the *e*-beam irradiation of carbon soot particles and graphite (5). Popular models of these nanostructures could be described as nested Russian doll structures with concentric shells of large fullerene-like molecules.

Despite the appeal of the Russian doll model, defects of various forms have been apparent in published HREM images of carbon nanostructures (mixtures of tubes and onions). Amorphous carbon deposits have been noted on both the outer surface and in the center of the nanotubes (3, 4). Discontinued graphite sheets can be found in both the nanotubes (4) and onions (5) by tracing of the lattice fringes. Dislocations have been discussed by Harris and colleagues (6). In one case, the transmission electron microscope (TEM) image of an uncapped tube viewed end-on resembles a spiral more than concentric cylinders (7). Even when defects are present, our computer simulations (Fig. 1) show that edge dislocations parallel to the tube axis are difficult to observe when they are projected normal to the tube axes (because of the morphology, most of the nanotubes can only be viewed along this direction). Thus, the observation of the same number of HREM lattice fringes on either side of the hollow center does not guarantee a

perfect, nested fullerene structure.

Because of the limitations of HREM, we have sought to address the structural question through bulk physical and chemical properties. The premise of our approach is that the distance between adjacent shells in nested structures would be relatively unaffected by pressure (in contrast to the high interlayer compressibility in graphite), and that the intershell “galleries” within a nested nanostructure would be inaccessible to intercalation (just as is the interior of a C₆₀ molecule).

The material used in this study was synthesized by the method of Ebbesen and Ajayan (4) and included samples prepared at AT&T and Rice University. The samples contained mostly tubes and onions, as shown by the representative HREM pictures in Fig. 2. The ratio of tubes to onions varied among experiments. The smallest nanotubes had two concentric graphitic shells. Most contained 20 to 30 layers with an intershell distance of ~3.4 Å, inner diameters of ~20 to 30 Å, and lengths greater than 1 μm. The ends always appeared to be closed in HREM images.

A powder x-ray diffraction pattern of a typical sample is shown in Fig. 3A. The pattern can be indexed on the basis of the hexagonal close-packed “graphite” unit cell with the *c* axis enlarged from 6.71 to 6.88 Å while the same C–C bond length is kept. This pattern is consistent with the findings of an earlier report (8) and is remarkably similar to the pattern of turbostratic graphite (9, 10). The symmetrical (002) peak probes the average intershell spacing within each nanoparticle and is broadened from the finite number of layers in a single particle. The average interlayer spacing of 3.44 Å is 0.09 Å larger than that of crystalline graphite and reflects the lack of positional correlation between carbon atoms in different

AT&T Bell Laboratories, Murray Hill, NJ 07974, USA.

shells of the same nanostructure (11), as expected from the geometry. The average coherence along the radial direction deduced from the width of the (002) Bragg peak is ~ 140 Å (~ 40 layers), in reasonable agreement with the HREM result. The (hk0) peaks are strongly asymmetrical with a "sawtooth" shape, and (hk ℓ) reflections are nearly absent. The asymmetry reflects the lack of correlations between carbon atoms in different layers.

The average radial compressibility of the nanostructures can be calculated from the pressure-induced shift in d_{002} , which measures the interlayer separation. The interlayer compressibility of graphite is independent of the in-plane C–C distance. However, for a closed, cylindrical graphite sheet, contraction must shorten C–C bonds, and for concentric cylinders it can be shown that

$$\frac{\Delta d_{(002)}}{d_{(002)}} = \frac{\Delta a}{a}$$

where a is the C–C bond length (12). Therefore, if the nanostructures are nested, they should be as incompressible radi-

ally as graphite is in the ab plane.

High-pressure x-ray diffraction patterns were collected by a position-sensitive detector, with 0.687 Å synchrotron radiation and a diamond anvil cell at the National Synchrotron Light Source beam line X7A. The inset to Fig. 3A shows d_{002} as a function of the applied hydrostatic pressure. The (002) reflection remained symmetric and changed from 3.41 Å at 1 bar to 3.30 Å at 10.2 kbar, four times the full width at half maximum of the Bragg peak at 1 bar. A linear fit to the data up to 10 kbar yields a radial compressibility ($\delta \ln a / \delta P$, where a is the C–C bond length) of $3.1 \times 10^{-3}/\text{kbar}$, comparable to the value reported for the c -axis compressibility of graphite ($2.7 \times 10^{-3}/\text{kbar}$) (13). This value is an order of magnitude larger than the $1.3 \times 10^{-4}/\text{kbar}$ in-plane compressibility of graphite (14), counter to the expectations of the nested structure.

The carbon nanostructures were reacted with K and Rb under conditions similar to those leading to intercalation in graphite and C_{60} . In a typical reaction, the sample was reacted with an excess of alkali metal in an evacuated pyrex ampoule at 350°C for a few days. Following the reaction, the weight uptake was measured in a He-filled dry box. For both K and Rb, the weight gain indicated an overall composition of MC_8 , and the material had a dark, gold-tinted color. The stoichiometry and

color of the reacted material are the same as the corresponding saturated, stage-1 graphite intercalation compounds (15). The x-ray powder diffraction pattern of a sample saturated with Rb is shown in Fig. 3B. The Bragg peaks of the pristine nanostructures disappeared completely, and a new set of diffraction peaks occurred, which can be indexed on a hexagonal unit cell with $a = 4.95$ and $c = 5.68$ Å. As in the unreacted sample, the (00 ℓ) reflections are relatively sharp, whereas the (hk0) reflections have the characteristic asymmetric sawtooth line shape. The hexagonal unit cell is essentially the same as that of the stage-1 Rb intercalated graphite RbC_8 , when the ordering of the alkali metal is ignored (15). The 5.68 Å c axis lattice parameter corresponds to a 2.3 Å expansion in the intershell spacing.

Upon exposure to air, the color of the alkali metal-reacted sample returned to the black color of the unreacted material. The dominant 3.44 Å (002) peak observed in the pristine material also reappeared in the x-ray diffraction pattern (but much broader and weaker than before reaction). The result indicates deintercalation upon air exposure. A deintercalated potassium-doped sample was examined by TEM, and representative HREM micrographs are shown in Fig. 4 (HREM pictures of the nanostructures from the same batch before reaction to alkali metal are shown in Fig. 2). In contrast to the well-ordered and smooth lattice fringes observed in the unreacted sample, the carbon layers in the air-exposed samples were disordered, to the extent that no clear lattice fringes were resolved in some regions. The outer layers of the nanotubes were jagged with many missing fragments. In some cases, a section of the tube was relatively well ordered and others were disordered. Even in the ordered section, high concentrations of edge dislocations were observed on the outer layers, exposing the interlayer van der Waals galleries. Although continuous layers exceeding 1000 Å can still be traced in some nanotubes, most of the carbon layers appeared to be about 100 Å in length along the tube axes. On average, the outer shells were more disordered and had a larger intershell spacing than the intershells. The caps that often appeared to be perfect in the unreacted nanotubes were found to be either amorphous or highly disordered. The onions were as disordered as the tubes. Many highly defective tubes appeared to be decorated with small onions on the outer surfaces. This appearance suggests that these onions could have been formed from the fragmented carbon monolayers.

In the analogous graphite and C_{60} systems, the van der Waals galleries between adjacent carbon sheets or C_{60} molecules

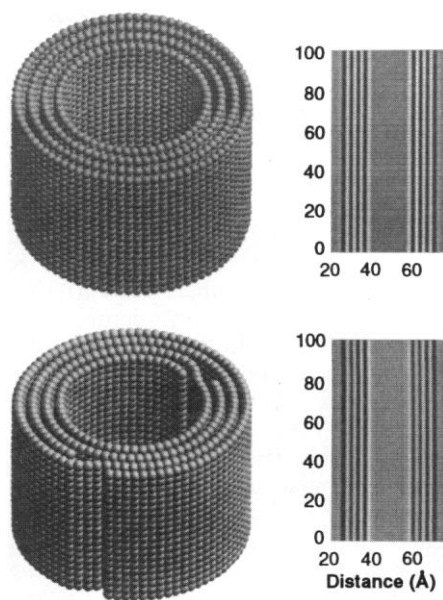


Fig. 1. Simulated real space HREM images of (top) a defect-free tube and (bottom) a tube with edge dislocations. For ease of modeling, the tubes extend only 20 C–C distances along the tube axes, and the carbon atoms are in rectangular arrays rather than six-member rings. Edge dislocations are parallel to the tube axis. HREM images were simulated with Cerius software (Molecular Simulation, Waltham, Massachusetts) for tubes with different numbers of layers and edge dislocations. Except in the case of a two-layer tube, the number of lattice fringes on each side of the hollow center are always the same when projected normal to the tube axes. A 200-KeV beam voltage and a -290 Å defocus were used.

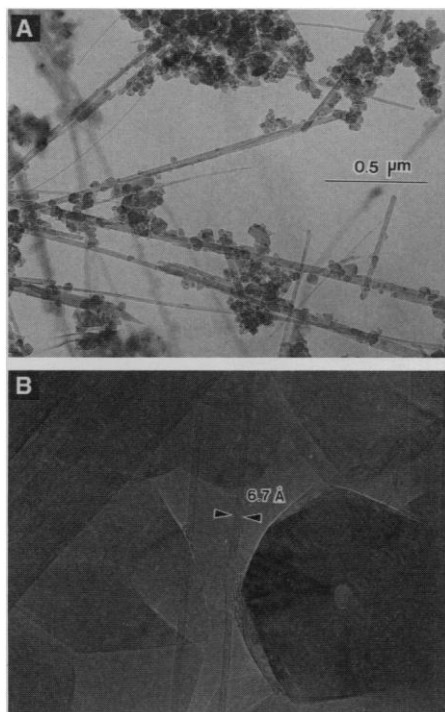
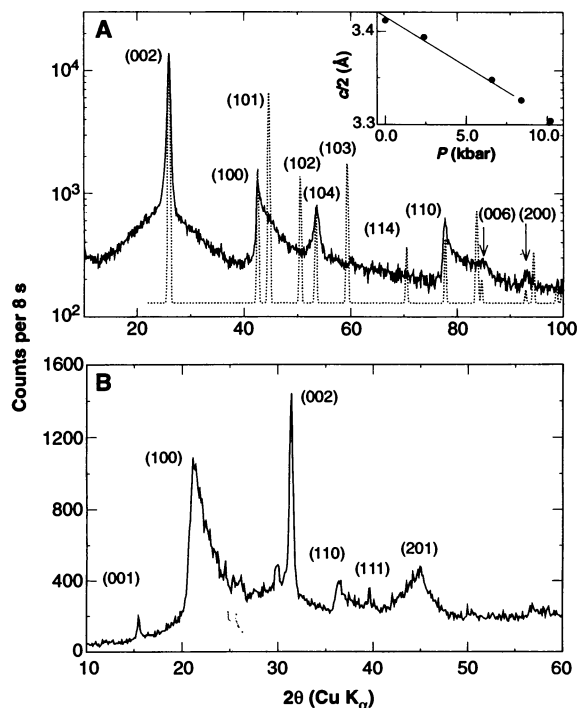


Fig. 2. Representative HREM images of the carbon nanostructures used in this study. (A) Overall distribution of nanotubes and nanoparticles. (B) High-magnification micrograph.

Fig. 3. (A) An x-ray diffraction from a sample consisting predominately of carbon nanostructures. A calculated diffraction pattern of "graphite" with the interlayer spacing set to 6.87 Å (versus 6.696 Å) is shown for comparison. The broad feature under the sharp (002) peak is from the diffuse scattering intensities of the glass capillary used as a sample container. The inset shows the pressure dependence of the average interlayer spacing (c , c -axis lattice parameter). (B) An x-ray diffraction of the sample shown in (A) after reaction with excess Rb metal.



provide the only diffusion pathway and the equilibrium sites for the intercalants. The carbon six- and five-member rings are impenetrable to alkali metal atoms. The evaporation of potassium on the graphite (001) surface results in intercalation only if a large number of surface defects are present (16). For a nested structure, point defects alone are insufficient to account for the lattice expansion on intercalation and the large radial compressibility. Instead, extended defects are called for that would allow adjacent layers to slip over each other.

The defect argument is also supported by the drastic change of morphology observed in the nanostructures after reaction and air exposure. Previous chemistry showed that capped nanotubes could be thinned and opened when heated in an oxidizing environment (air or CO_2) (17, 18). However, it is unlikely that the nanostructures can be ruptured either from reaction with K or Rb under the mild reaction conditions of our experiment (350°C in vacuum) or exposure to air after the reaction, because closed tubes or onions should be at least as robust as fullerene molecules, which do not rupture under similar reaction conditions. On the basis of the morphology of the nanostructures after reaction and exposure to air, the defect concentration must be large in the pristine material, because most of the carbon shells are only about 100 Å in length along the tube axes. Furthermore, the caps on nanotubes are not immune to defects.

The stability of tubular, spherical, or both types of nonclosed concentric structures compared to that of their two-dimensional counterpart can be provided by the

gain in the van der Waals attractive energy over the energy needed to bend the layer. According to empirical estimates, there is a binding energy between individual sheets of two-dimensional graphite of about 1 to 2 kcal/mol per carbon atom due to the van der Waals interactions (19, 20). Quantum molecular dynamics simulations of open cylinders (21) indicate that the strain energies (22) per carbon atom fall below 2 kcal/mol at a cylinder radius of about 6 Å. Given that the inner and outer sheets of the jelly roll have van der Waals interactions on only one side and that the interlayer separation is somewhat greater than for graphite, the 20 to 30 Å inner tube diameter observed by HREM is reasonable. A single 1- μm -square sheet of graphite spiral wound with an inner diameter of 20 Å and an interlayer spacing of 3.44 Å would yield a tube with about 28 layers.

Although the compressibility and the chemical reactivity toward alkali metals of the carbon nanostructures are similar to that of turbostratic graphite, the magnetic properties, as characterized by dc magnetization and electron spin resonance (ESR) measurements, are distinctly different. The density of spins measured by ESR is less than that in graphite by at least an order of magnitude and similar to that in C_{60} . The g values are 2.004 (graphite), 2.000 (tubes), and 2.000 (C_{60}) (23). Direct-current magnetization measurements of the carbon nanostructures (0.5 T in a superconducting quantum interference detector) at 300 K give a powder-averaged susceptibility, χ , of -105×10^{-6} electromagnetic units (emu) per mole of carbon, significantly

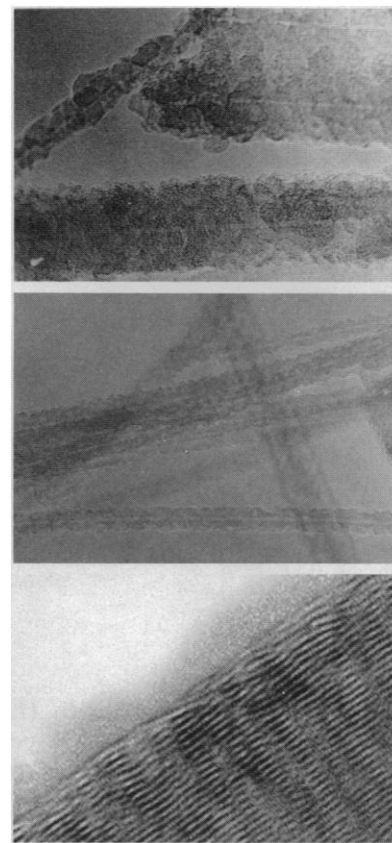


Fig. 4. HREM images of the carbon nanostructure sample after reaction to K and air exposure. (HREM pictures of the sample from the same batch before reaction are shown in Fig. 2.)

more diamagnetic than the corresponding values of -37.3×10^{-6} and -86.2×10^{-6} emu/mol for carbon black (turbostratic by x-ray) and highly oriented pyrolytic graphite (HOPG), respectively (24).

Although carbon nanostructures have morphologies and electronic properties that are distinct from other forms of carbon, they are highly defective and have a local structure similar to that of turbostratic graphite. The presence of at least some perfect, nested structures cannot be ruled out, but the overwhelming majority of the material is better described as a "paper-mache" of small graphitic sheets, rather than a nested Russian doll. This type of model has been proposed for carbon black spheroids (25).

REFERENCES AND NOTES

- W. Kratschmer, L. D. Lamb, K. Fostiropoulos, D. R. Huffman, *Nature* **347**, 354 (1990).
- R. E. Haufler et al., *J. Phys. Chem.* **94**, 8634 (1990).
- S. Iijima, *Nature* **354**, 56 (1992).
- T. W. Ebbesen and P. M. Ajayan, *ibid.* **358**, 16 (1992).
- D. Ugarte, *ibid.* **359**, 707 (1992).
- P. J. F. Harris, M. L. H. Green, S. C. Tsang, *J. Chem. Soc. Faraday Trans.* **89**, 1189 (1993).
- V. P. Dravid et al., *Science* **259**, 1601 (1993).

8. Y. Saito, T. Yoshikawa, S. Banndow, M. Tomita, T. Hayashi, *Phys. Rev. B* **48**, 1907 (1993).
9. W. Ruland, in *Chemistry and Physics of Carbon*, P. L. Walker Jr., Ed. (Dekker, New York, 1968), p. 1.
10. B. E. Warren, *Phys. Rev.* **59**, 693 (1941); J. Biscoe and B. E. Warren, *Appl. Phys.* **13**, 364 (1942).
11. R. E. Franklin, *Acta Crystallogr.* **3**, 107 (1950); *ibid.* **4**, 253 (1950).
12. The relation between radial and longitudinal compressibilities is derived here for a zigzag (n , 0) tube. In this geometry, the radius of the i th shell of the tube, r_i , is equal to $n_i\sqrt{3}a/2\pi$, where n_i is the number of carbon atoms along the circumference of the i th shell and a is the C—C bond length. For concentric tubes, $d_{002} = r_{i+1} - r_i = (n_{i+1} - n_i)\sqrt{3}a/2\pi$. Assuming that the change in the bond length is the same in every shell, one can arrive at the conclusion that $\Delta d_{002}/d_{002} = \Delta a/a$.
13. H. Zabel, in *Graphite Intercalation Compounds*, H. Zabel and S. A. Solin, Eds. (Springer-Verlag, Berlin, 1990), p. 101.
14. The ab plane linear compressibility of graphite was obtained by a linear fit to in-plane lattice parameter versus pressure data of R. W. Lynch and H. G. Drickamer [*J. Chem. Phys.* **44**, 181 (1966)] to 20 kbar.
15. M. S. Dresselhaus and G. Dresselhaus, *Adv. Phys.* **30**, 139 (1981).
16. N. J. Wu and A. Ignatiev, *Phys. Rev. B* **28**, 7288 (1983).
17. S. C. Tsang, P. J. F. Harris, M. L. H. Green, *Nature* **362**, 520 (1993).
18. P. M. Ajayan *et al.*, *ibid.*, p. 522.
19. L. A. Girifalco and R. A. Lad, *J. Chem. Phys.* **25**, 693 (1956).
20. S. W. Benson, *Thermochemical Kinetics* (Wiley, New York, 1976).
21. G. B. Adams, O. F. Sankey, J. B. Page, M. O'Keefe, D. A. Drabold, *Science* **256**, 1792 (1992).
22. R. C. Haddon, *ibid.* **261**, 1545 (1993).
23. S. H. Glarum, S. J. Duclos, R. C. Haddon, *J. Am. Chem. Soc.* **114**, 1996 (1992).
24. The origin of the enhanced diamagnetism will be discussed in a separate paper (A. P. Ramirez *et al.*, in preparation).
25. R. D. Heidenreich, W. M. Hess, L. L. Ban, *J. Appl. Crystallogr.* **1**, 1 (1968).
26. We thank M. J. Rosseinsky, R. Felder, J. E. Fischer, P. A. Heiney, R. Tycko, G. Dabbagh, D. J. Eaglesham, and A. J. Lovering for useful discussions and technical assistance; J. E. Fischer for providing the HOPG sample; D. E. Cox for the use of his apparatus at Beam Line X7A, National Synchrotron Light Source (NSLS); and R. E. Smalley for samples and comments on the manuscripts. NSLS is supported by the U.S. Department of Energy, Division of Materials Sciences and Division of Chemical Sciences.

24 November 1993; accepted 1 February 1994

Changes in Atmospheric Circulation and Ocean Ice Cover over the North Atlantic During the Last 41,000 Years

P. A. Mayewski,* L. D. Meeker,† S. Whitlow, M. S. Twickler, M. C. Morrison, P. Bloomfield, G. C. Bond, R. B. Alley, A. J. Gow, P. M. Grootes, D. A. Meese, M. Ram, K. C. Taylor, W. Wumkes

High-resolution, continuous multivariate chemical records from a central Greenland ice core provide a sensitive measure of climate change and chemical composition of the atmosphere over the last 41,000 years. These chemical series reveal a record of change in the relative size and intensity of the circulation system that transported air masses to Greenland [defined here as the polar circulation index (PCI)] and in the extent of ocean ice cover. Massive iceberg discharge events previously defined from the marine record are correlated with notable expansions of ocean ice cover and increases in PCI. During stadials without discharge events, ocean ice cover appears to reach some common maximum level. The massive aerosol loadings and dramatic variations in ocean ice cover documented in ice cores should be included in climate modeling.

During the last glaciation, the North Atlantic region experienced major changes in climate relative to the Holocene (the most recent 10,000 years). The most obvious and

dramatic of these changes consisted of variable length stadial (cold) and interstadial (milder) periods. The major ion series (1) collected as part of the Greenland Ice Sheet Project Two (GISP2) (72.6° N, 38.5° W, 3200-m elevation) provide a particularly sensitive monitor of these events. This multivariate suite of time series reveals a record of variability in the major soluble constituents of the atmosphere over Greenland (2, 3) that can be used to interpret response to climate change (changes in atmospheric circulation and ocean ice cover extent) and the potential influence of several major climate forcing agents (dust loading, ocean ice cover, and ice sheet stability).

We analyzed the GISP2 calcium, chloride, sulfate, sodium, magnesium, potassium, ammonium, and nitrate ion series covering the last 41,000 years (Fig. 1). A previously identified antiphase relation between oxygen isotopes and dust (4, 5) holds, to a variable degree, between oxygen isotopes and many ion species (Fig. 1). It is

the common features among the multivariate ion species and the contrasting divergence from that commonality by individual ion records that provide the detailed view of atmospheric circulation over the North Atlantic that we discuss below.

Because the two primary sources for chemical species transported to the Greenland atmosphere are terrestrial dusts and marine surfaces (2), we focus here on changes in the chemical series that monitor these sources. Quantities for these two sources (Fig. 2) were estimated by partitioning (6) calcium, chloride, sulfate, sodium, magnesium, and potassium into sea salt and excess (total minus estimated sea salt) contributions. Excess quantities were then combined to provide an estimate of terrestrial dust. Stadials (low oxygen isotope events) are characterized by synchronous increases in both dust and sea salt, whereas relatively low concentrations of both components are typical of the interstadials (high oxygen isotope events).

Neither ammonium nor nitrate concentrations (Fig. 1) are accounted for in the dust and sea salt estimates. These two species represent less than 8% of the total soluble ionic loading of the atmosphere during the pre-Holocene and display only subtle to minimal variation in that portion of the record. Because interpretation of the concentration records is not straightforward (7), our discussion is limited to the remaining six GISP2 ion series.

Dust and sea salt concentrations differed significantly during the Holocene, stadials, and interstadials [including during the Bolling/Allerod (B/A)]: 11 and 17, 267 and 165, and 52 and 72 parts per billion (ppb), respectively. Ionic balance determinations revealed other differences. During the glacial period, at least 50% of the calcium was in the form of CaCO_3 , with the remainder of the calcium and other cations in the form of compounds such as NaCl , NaNO_3 , CaSO_4 , and $(\text{NH}_4)_2\text{SO}_4$ (3). This distribution is a significant departure from the

P. A. Mayewski, L. D. Meeker, S. Whitlow, M. S. Twickler, M. C. Morrison, Glacier Research Group, Institute for the Study of Earth, Oceans, and Space, University of New Hampshire, Durham, NH 03824, USA.

P. Bloomfield, Department of Statistics, North Carolina State University, Raleigh, NC 27695-8203, USA.

G. C. Bond, Lamont-Doherty Earth Observatory, Palisades, NY 10964, USA.

R. B. Alley, Earth System Science Center and Department of Geosciences, Pennsylvania State University, University Park, PA 16802, USA.

A. J. Gow and D. A. Meese, Cold Regions Research and Engineering Laboratory, Hanover, NH 03755, USA.

P. M. Grootes, Quaternary Isotope Laboratory, University of Washington, Seattle, WA 98195, USA.

M. Ram, Department of Physics, University of Buffalo, Amherst, NY 14260, USA.

K. C. Taylor, Desert Research Institute, University of Nevada System, Reno, NV 89506, USA.

W. Wumkes, Polar Ice Coring Office, University of Alaska, Fairbanks, AK 99775, USA.

*To whom correspondence should be addressed.

†Also at Department of Mathematics, University of New Hampshire, Durham, NH 03824, USA.